2Q PROGRESS REPORT

Siemens-Masdar Institute Collaborative Research

Automated, Comfort-Constrained Demand Response Using Thermal Energy Storage

Project Period: 10 July 2013 to 31 January 2013

Principal Investigators at Masdar Institute: Peter Armstrong and Afshin Afshari

EXECUTIVE SUMMARY

Work in the first two quarters has focused on development and testing of model identification for transient thermal response, Tasks 2 and 4. Substantial work to prepare a test building has also been completed in Task 6.

A general formulation of the demand response problem involving cool storage in the building structure is given. Two transient thermal response models are embedded in the general formulation, one for the occupied zone and one for TABS element connected with that zone. We have developed a method of estimating a comprehensive room transfer function (CRTF) from the TRNSYS zone model. These results are presented in Research Sections 1 and 2.

A new representation of heat pump and chiller performance has been formulated and tested using performance maps generated by detailed simulation. The representation is based on first principles models of irreversibilities in heat transfer, fluid transport and motors and drives. Results are presented in Research Section 3.

The preferred demonstration venue, MIST 1B is still under construction and will probably be occupied August 2013 with commissioning still underway (Potter 2013). This is not the ideal situation for initial testing of the model identification procedure. Efforts are therefore underway to upgrade the BMS of the *Masdar Field Station* (MFS), characterize its leakiness and transient thermal response, and modify parts of the air and hydronic distribution systems. eQuest and TRNSYS models of the MFS have been developed. Progress in these areas is reported in Research Section 4.

The demand response (DR) monitoring part of Task 6 will begin in the 4th quarter so that summer performance can be observed in 2013 rather than 2014. Task 1 has been rescheduled to begin in the 4th quarter after live testing of DR and model predictive control is underway. In the next quarter we expect to complete Tasks 2, 3, and 4 so that testing of demand response can begin by June in the MFS.

INTRODUCTION

Background

Demand response (DR) is a key Smart Grids/Smart Buildings (SGSB) function. In Summer-peaking regions cooling loads contribute to and coincide broadly with system peak. Simple peak shaving is an ineffective DR strategy in this context because of its immediate and often unacceptable impact on thermal comfort. The alternative is to shift cooling load to off-peak (e.g., via pre-cooling during early morning hours) using thermal storage in order to prevent or attenuate the deterioration of indoor thermal conditions. The thermal capacitance of buildings is a potential low-cost DR storage resource. To be useful, precooling, reduction of peak cooling rate, and restoration to preferred conditions in occupied zones must be automated in order to adjust to envelope/systems dynamics and end-use profiles. The transient thermal response to cooling load excitations (internal gains, solar, outdoor temperature and RH, and cooling effect) and to cooling effect dispatched to zone or TABS, must be quickly, accurately and automatically characterized so that large and predictable load-shifts can be achieved within comfort constraints. DR has a large potential impact in terms of marginal cost of supply, carbon emissions and generation/transmission capacity expansion requirements. However the cooling load related DR resource is highly distributed such that the costs per customer—both implementation and occupant acceptance—must be low. The project addresses both of these costs head on.

Objective and Approach

The project objective is to develop methods to quickly and reliably identify zone models that accurately predict zone air and mean radiant temperatures (MRT) under strong transient conditions. Specific objectives include 1) show that test set forecast residuals are consistently closer to training set residuals when the UA and alternating roots constraints are applied to a wide variety of simulated buildings and zones; 2) demonstrate 100% convergence for 3rd- or higher order models with both simulated (noise added) and real data; and 3) demonstrate DR control in MIST 1A or 1B test zones. Progress to date (first 6 months) is reported below.

RESEARCH 1: MPC FORMULATION FOR DR

The problem is to minimize the daily sum (N=24) of hourly operating costs under time-of-use pricing, $E(t)$.

$$J = \sum_{t=1}^{N} \frac{E(t)(Q_u(t) + Q_z(t))\Delta t}{COP(Q(t), T_x(t), T_{ss}(t))}$$

where $Q_u(t)$ = TABS charging rate, $Q_z(t)$ = direct cooling rate, $Q(t) = Q_u(t) + Q_z(t)$, and COP is the ratio of total capacity, $Q(t)$, to cooling *system* input power, $W(t) = Q(t)/COP(t)$. Note $W(t)\Delta t$ is the energy used in time step t and $E(t)W(t)\Delta t$ is the cost of that energy. We usually assume $E(t)$ $t = 1{:}24$ is announced at around midnight.

The zone comfort constraints for $t = 1{:}24$ (assuming hourly steps) are given by

$$T_{z,\min}(t) \le T_z(t) \le T_{z,\max}(t)$$

Zone temperature, T_z, is given in terms of current and past zone heat gains and cooling rates as well as current and past outdoor and adjacent zone temperatures and past zone temperatures:

$$T_z = f(Q_z + Q_{IG}, T_{xw}, T_{aw})$$

Similarly the under-slab temperature is given in terms of recent charging rates and zone and under-slab temperatures:

$$T_u = f(Q_u, T_z)$$

Evaporating temperature depends on capacity, flow rate, and heat exchanger parameters as follows:

$$Q_u = \varepsilon_u C_{umin}(T_u - T_{ss}) \geq 0$$

$$Q_z = \varepsilon_z C_{zmin}(T_z - T_{ss}) \geq 0$$

There are 48 optimization variables, the 24 hourly values of cooling delivered to TABS, Q_u, and the 24 hourly values of cooling delivered to the zone via RCP, chilled beam, EFC, or DX-fan-coil, Q_z. The constrained minimization problem will be solved for all hours using the recent past measured values of all T and Q and the 24-hour-ahead forecasts, t = 2:24, of the exogenous variables:

T_x = heat rejection (usually dry-bulb) temperature
T_{xw} = sol-air temperatures on exterior walls
T_{aw} = room temperatures of adjacent zones, and
Q_{IG} = zone internal and solar gains.

Information flow for the 24-hour-ahead MPC control is shown in Figure 1. In hours when Q_u and Q_z are both non-zero we have two possible formulations. 1) Load-side flow rates are adjusted such that the resulting T_{ss} minimizes system power for the hour. 2) The hour is divided and load-side flow rates are adjusted such that T_{ss} is constant over the hour and fan/pump energy is minimized. To minimize energy use, rather than cost, the 24 hourly energy prices, $E(t)$, can be set to one.

For each hour's trial values of Q_u and Q_z the value of T_{ss} that minimizes system power is found by interval bisection where upper bound $T_{ss} = T_u$ for precooling or T_z for direct cooling and lower bound $T_{ss} = T_u - Q_u/C_{umin}$ for precooling or $T_z - Q_z/C_{zmin}$ for direct cooling and where C_{umin} and C_{zmin} are minimum thermal capacitance rates of TABS pump and DX-fan-coil

The control method may be extended to multiple zones as shown schematically in Figure 2.

To demonstrate the precooling strategy in the Masdar Field Station we will solve the optimal precooling problem every half hour on a PC and control the indoor unit fans, pumps and hydronic valves directly from the PC. To control outdoor unit capacity, the evaporating temperature (SST) command will be sent to the plant VRF unit which will control EXV settings, compressor speeds and condenser fan speed in the usual way as shown in Figure 2.

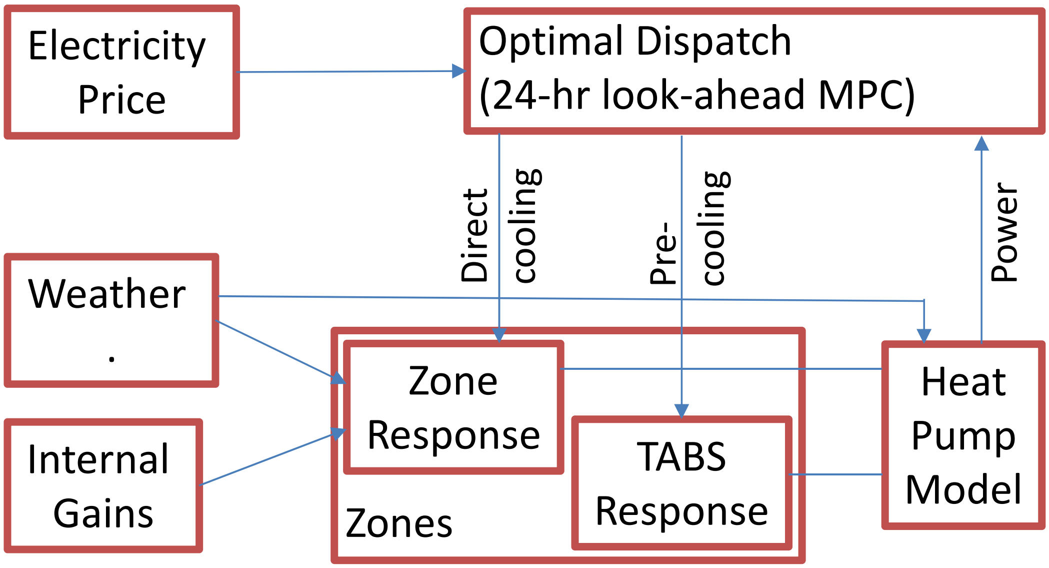

Figure 1: Information Flow for 24-Hour-Ahead Optimal Dispatch of Direct and Precooling.

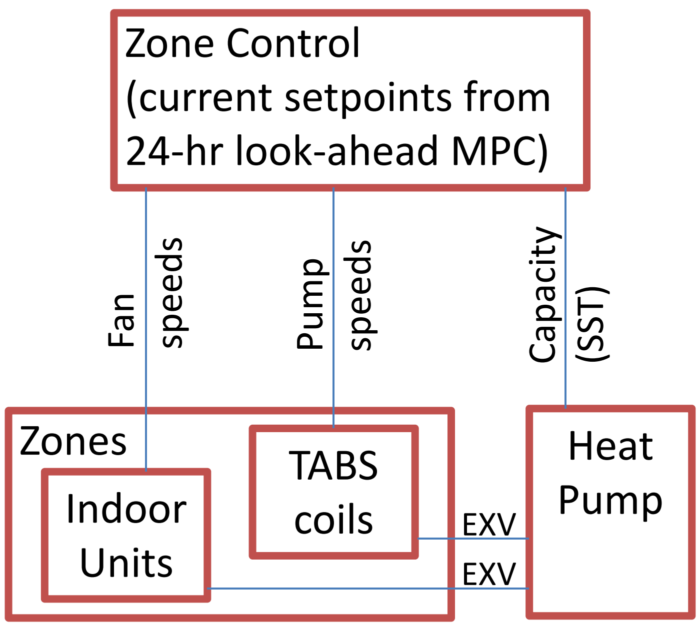

Figure 2: Direct and Precooling Rates Using Fan- and Pump-Speed Setpoints Commanded by MPC.

Research 2: Identification of Transient Thermal Response Model

A very computationally efficient representation of transient thermal response is needed to make optimal model-predictive control feasible. One such representation is the comprehensive room transfer function (Seem 1987). Seem describes methods to estimate CRTF coefficients from the engineering description of a zone that can be modeled by coupled conduction transfer functions (CTFs). For MPC to become practical it will be necessary to estimate CRTFs from a standard simulation model or from careful observations of building thermal response. In the latter case the forcing functions are necessarily a mixture of natural excitations (weather) and induced excitations (heating or cooling of zones, exterior shading of direct solar radiation, etc.). We start with the simulation model case.

In heat transfer, a transfer function is defined as a recursive difference equation relating the outputs of a linear, time-invariant thermal system to a time series of current and past inputs, as well as a time series of past outputs. A Comprehensive Room Transfer Function (CRTF) is a single transfer function with multiple boundary conditions that models all transient heat transfer in a room or zone and its enclosing walls. Estimating the CRTF of the MFS zones is necessary in order to quickly, accurately, and automatically characterize the transient thermal response of the system, so that comfort constraints can be maintained even in the presence of large load-shifts and weather changes.

There are three main ways to obtain the CRTF for a system:

- From the conduction transfer functions of all walls enclosing the zone.
- Measured excitation and response of the system (Armstrong 2006).
- Excitation and response of a TRNSYS model (or other detailed building model).

The investigation of the MFS CRTFs was begun by analyzing a single zone. The zone was simplified to consist of just four walls, the ground, and the roof, with no windows or other building elements. This simple single zone is used to establish efficient and robust methodology for determining the CRTF, after which this methodology can be directly applied to the detailed TRNSYS MFS model.

The CRTF uses a star network to approximately model radiant and convective heat transfer within a zone. We formulate the CRTF with the star temperature, T_{star}, as the dependent variable. The star temperature is the temperature of a fictitious node connected to each wall and the air node. The star network (Seem, 1987) approximately models long-wave radiation exchange amongst the zone inside surfaces and the convective heat fluxes from the inside surfaces to the air node air. This formulation results in the following as yet unconstrained CRTF model:

$$T_{star}(t) = \sum_{k=1}^{n} \phi_k T_{star}(t-k) + \sum_{i=1}^{w}\sum_{k=0}^{n} \phi_{i(n+1)+k} T_{wall,i}(t-k) + \sum_{k=0}^{n} \phi_{(w+1)(n+1)+k}\, \dot{Q}_{conv}(t-k)$$
$$+ \sum_{k=0}^{n} \phi_{(w+2)(n+1)+k} \dot{Q}_{rad}(t-k) + u(t) \qquad (1)$$

where

n is the order of the system,

w is the number of walls in a zone (currently six) and i refers to the i^{th} wall,

T_{wall} is a uniform exogenous temperature at the outside of the i^{th} wall,

$\dot{Q}_{conv}$ is the convective heat input into a zone,

$\dot{Q}_{rad}$ is the radiative heat input into a zone,

ϕ is a vector of system coefficients that define the CRTF,

$u(t)$ is a vector of the residuals of the system.

Upon expanding the summations in the equation, it is apparent that the coefficients ϕ can be estimated by ordinary least squares regression. Note, as implicitly stated in Equation (1), that ϕ_0 = -1. In order to ensure that the regression yields physically sensible results, as well as to make the CRTF coefficients less sensitive to measurement error, thermodynamic constraints are applied to the model. These constraints are obtained from a thermal analysis of the system, and can be used to force the regressive model to abide by certain physical restraints that are known. The first such constraint is given by the thermal steady-state of the system as a whole, as described by Armstrong *et al* (2006):

$$Q_{conv} + Q_{rad} = \sum_{i=1}^{w} u_i (T_{wall,i} - T_{star}) \tag{2}$$

where u_i = UA_i is the conductance-area product of the i^{th} wall.

Therefore, by combining equations 1 and 2, the coefficients of the regressive model must abide by the following constraint:

$$\frac{\sum_{i=1}^{w}\sum_{k=0}^{n}\phi_{i(n+1)+k}}{\sum_{k=0}^{n}\phi_{(w+1)(n+1)+k}+\phi_{(w+2)(n+1)+k}} = \frac{\sum_{k=0}^{n}\phi_k}{\sum_{k=0}^{n}\phi_{(w+1)(n+1)+k}+\phi_{(w+2)(n+1)+k}} = \sum_{i=1}^{w} u_i \tag{3}$$

from which the common denominator may be removed to give

$$\sum_{i=1}^{w}\sum_{k=0}^{n}\phi_{i(n+1)+k} = \sum_{k=0}^{n}\phi_k \tag{4}$$

For example, a fourth order system with six walls should be constrained thus:

$$\sum_{k=5}^{34}\phi_k = 1 - \sum_{k=1}^{n}\phi_k \tag{5}$$

Using this constraint, we can define one of the coefficients in terms of the others, thus reducing the number of model coefficients by one, and forcing the model to abide by steady state heat transfer. The coefficient chosen to be eliminated is ϕ_5, the coefficient for the current temperature of wall 1. The reduced model now becomes:

$$\begin{aligned} T'_{star}(t) = {} & \sum_{k=1}^{n}\phi_k T'_{star}(t-k) + \sum_{k=n+1}^{2n}\phi_k T'_{wall,1}(t-k) + \sum_{i=2}^{w}\sum_{k=0}^{n}\phi_{i(n+1)+k-1} T'_{wall,i}(t-k) \\ & + \sum_{k=0}^{n}\phi_{(w+1)(n+1)+k-1}\,\dot{Q}'_{conv}(t-k) + \sum_{k=0}^{n}\phi_{(w+2)(n+1)+k-1}\dot{Q}'_{rad}(t-k) + u(t) \end{aligned} \tag{6}$$

where $X' = X - T_{wall,1}(t)$

With a sufficiently long and rich record of observed excitations and responses coefficients of the reduced model may be determined by regression. To do this, step excitations of all independent variables in the TRNSYS single zone model are individually applied. First, a wall's temperature is stepped up to 1°C from the initial condition of 0°C, and all other parameters (aside from air node temperature) are set to zero. The response of the system to this step excitation is recorded, and this procedure is repeated for all six walls. This is then also repeated with Q_{rad} and $Q_{conv.}$ The value of the step excitation of these two heat input terms is determined by trial and error as one that allows the air node temperature to reach 1°C at steady state. The step responses of the system are then used as training data to determine the coefficients of the CRTF.

Once the CRTF has been determined, it is tested. Abu Dhabi weather data from the year 2010 is applied to both the TRNSYS model and the CRTF, and the results are compared. Figure 3 shows the results of T_{room} for the yearlong simulation. The results show a strong agreement between the CRTF and TRNSYS results.

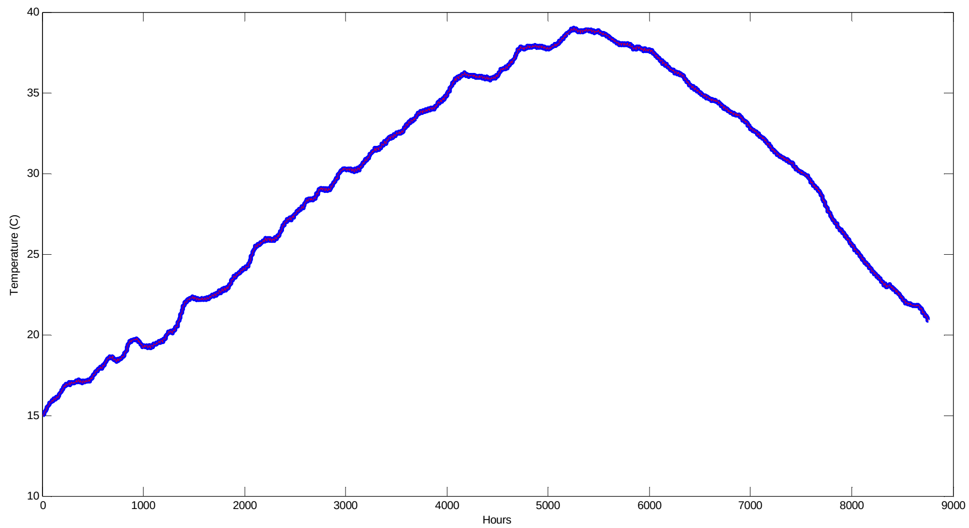

Figure 3: T_{room} Plot for Abu Dhabi Weather Data Simulation. CRTF results in red; TRNSYS results in blue.

Table 1 shows the t-statistic values for the coefficients of the CRTF for systems of order n=1 to n=4. The critical value of the t distribution for a significance level α=0.05 is $\pm$1.96.

Table 1: Values of t-statistic of Coefficients, RMSE and UA of CRTF for System Orders 1 to 4.

	n=1		n=2		n=3		n=4	
Variable	Coefficient	t-statistic	Coefficient	t-statistic	Coefficient	t-statistic	Coefficient	t-statistic
$T'_{star}(t-1)$	9.995×10^{-1}	9.2×10^{4}	1.722	4.4×10^{2}	1.832	2.4×10^{3}	2.412	2.4×10^{3}
$T'_{star}(t-2)$	-	-	-7.218×10^{-1}	-1.8×10^{2}	-6.814×10^{-1}	-5.0×10^{2}	-1.700	-9.2×10^{2}
$T'_{star}(t-3)$	-	-	-	-	-1.505×10^{-1}	-2.3×10^{2}	1.611×10^{-1}	2.3×10^{2}
$T'_{star}(t-4)$	-	-	-	-		-	1.267×10^{-1}	7.6×10^{2}
$T'_{wall,1}(t-1)$	4.705×10^{-4}	1.1	1.017×10^{-6}	4.1×10^{-3}	1.017×10^{-6}	5.0×10^{-2}	1.016×10^{-6}	4.5×10^{-1}
$T'_{wall,1}(t-2)$	-	-	1.150×10^{-4}	6.6×10^{-1}	1.329×10^{-5}	6.5×10^{-1}	1.270×10^{-5}	5.7
$T'_{wall,1}(t-3)$	-	-	-	-	-1.036×10^{-5}	-7.1×10^{-1}	1.758×10^{-5}	7.8
$T'_{wall,1}(t-4)$	-	-	-	-		-	-3.103×10^{-5}	-19.6
$T'_{wall,2}(t)$	4.163×10^{-10}	1.0×10^{-6}	4.163×10^{-10}	2.4×10^{-6}	4.162×10^{-10}	2.9×10^{-5}	4.162×10^{-10}	2.6×10^{-4}
$T'_{wall,2}(t-1)$	1.042×10^{-4}	2.5×10^{-1}	1.017×10^{-6}	4.1×10^{-3}	1.017×10^{-6}	5.0×10^{-2}	1.016×10^{-6}	4.5×10^{-1}
$T'_{wall,2}(t-2)$	-	-	2.685×10^{-5}	1.5×10^{-1}	1.329×10^{-5}	6.5×10^{-1}	1.270×10^{-5}	5.7
$T'_{wall,2}(t-3)$	-	-	-	-	-1.281×10^{-5}	-8.8×10^{-1}	1.758×10^{-5}	7.8
$T'_{wall,2}(t-4)$	-	-	-	-		-	-3.115×10^{-5}	-19.6
$T'_{wall,3}(t)$	4.163×10^{10}	1.0×10^{-6}	4.163×10^{-10}	2.4×10^{-6}	4.163×10^{-10}	2.9×10^{-5}	4.163×10^{-10}	2.6×10^{-4}
$T'_{wall,3}(t-1)$	1.042×10^{-4}	2.5×10^{-1}	1.017×10^{-6}	4.1×10^{-3}	1.017×10^{-6}	4.950×10^{-2}	1.016×10^{-6}	4.5×10^{-1}
$T'_{wall,3}(t-2)$	-	-	2.685×10^{-5}	1.5×10^{-1}	1.329×10^{-5}	6.5×10^{-1}	1.270×10^{-5}	5.7
$T'_{wall,3}(t-3)$	-	-	-	-	-1.281×10^{-5}	-8.8×10^{-1}	1.758×10^{-5}	7.8
$T'_{wall,3}(t-4)$	-	-	-	-		-	-3.115×10^{-5}	-19.6
$T'_{wall,4}(t)$	4.163E-10	1.0×10^{-6}	4.163×10^{-10}	2.4×10^{-6}	4.163×10^{-10}	2.9×10^{-5}	4.163×10^{-10}	2.6×10^{-4}
$T'_{wall,4}(t-1)$	1.042E-04	2.5×10^{-1}	1.017×10^{-6}	4.1×10^{-3}	1.017×10^{-6}	4.950×10^{-2}	1.016×10^{-6}	4.5×10^{-1}
$T'_{wall,4}(t-2)$	-	-	2.685×10^{-5}	1.5×10^{-1}	1.329×10^{-5}	6.5×10^{-1}	1.270×10^{-5}	5.7
$T'_{wall,4}(t-3)$	-	-	-	-	-1.281×10^{-5}	-8.8×10^{-1}	1.758×10^{-5}	7.8
$T'_{wall,4}(t-4)$	-	-	-	-		-	-3.115×10^{-5}	-19.6
$T'_{wall,5}(t)$	6.788E-08	1.6×10^{-4}	6.788×10^{-8}	3.9×10^{-4}	6.788×10^{-8}	4.7×10^{-3}	6.788×10^{-8}	4.3×10^{-2}
$T'_{wall,5}(t-1)$	2.554E-04	6.2×10^{-1}	2.122×10^{-5}	8.6×10^{-2}	2.121×10^{-5}	1.0	2.117×10^{-5}	9.4
$T'_{wall,5}(t-2)$	-	-	4.700×10^{-5}	2.7×10^{-1}	1.148×10^{-4}	5.6	1.025×10^{-4}	45.7
$T'_{wall,5}(t-3)$	-	-	-	-	-1.325×10^{-4}	-9.1	2.137×10^{-5}	9.5
$T'_{wall,5}(t-4)$	-	-	-	-		-	-1.449×10^{-4}	-92.0
$T'_{wall,6}(t)$	4.717E-11	1.1×10^{-7}	4.717×10^{-11}	2.7×10^{-7}	4.714×10^{-11}	3.2×10^{-6}	4.715×10^{-11}	3.0×10^{-5}
$T'_{wall,6}(t-1)$	3.339E-04	8.1×10^{-1}	1.704×10^{-7}	6.9×10^{-4}	1.704×10^{-7}	8.3×10^{-3}	1.704×10^{-7}	7.6×10^{-2}
$T'_{wall,6}(t-2)$	-	-	8.924×10^{-5}	5.1×10^{-1}	3.096×10^{-6}	1.5×10^{-1}	2.997×10^{-6}	1.3
$T'_{wall,6}(t-3)$	-	-	-	-	1.616×10^{-6}	1.1×10^{-1}	6.939×10^{-6}	3.1
$T'_{wall,6}(t-4)$	-	-	-	-		-	-9.530×10^{-6}	-6.0
$Q'_{conv}(t)$	1.590E-05	31.3	1.590×10^{-5}	74.1	1.590×10^{-5}	8.9×10^{2}	1.590×10^{-5}	1.1×10^{3}
$Q'_{conv}(t-1)$	-1.466E-05	-28.8	-1.707×10^{-5}	-55.1	-1.882×10^{-5}	-6.7×10^{2}	-2.804×10^{-5}	-1.7×10^{3}
$Q'_{conv}(t-2)$	-	-	1.493×10^{-6}	6.7	-1.522×10^{-6}	-52.7	8.691×10^{-6}	4.5×10^{2}
$Q'_{conv}(t-3)$	-	-	-	-	4.454×10^{-6}	2.4×10^{2}	5.163×10^{-6}	3.5×10^{2}
$Q'_{conv}(t-4)$	-	-	-	-		-	-1.708×10^{-6}	-1.1×10^{2}
$Q'_{rad}(t)$	3.243E-05	61.9	3.243×10^{-5}	1.5×10^{2}	3.243×10^{-5}	1.8×10^{3}	3.243×10^{-5}	2.2×10^{3}
$Q'_{rad}(t-1)$	-3.116E-05	-59.4	-2.504×10^{-5}	-74.1	-2.861×10^{-5}	-7.9×10^{2}	-4.744×10^{-5}	-1.4×10^{3}
$Q'_{rad}(t-2)$	-	-	-7.078×10^{-6}	-28.0	-3.149×10^{-5}	-9.3×10^{2}	-1.633×10^{-5}	-5.6×10^{2}
$Q'_{rad}(t-3)$	-	-	-	-	2.768×10^{-5}	1.3×10^{3}	4.736×10^{-5}	1.5×10^{3}
$Q'_{rad}(t-4)$	-	-	-	-		-	-1.603×10^{-5}	-5.7×10^{2}
RMSE	1.109×10^{-2}		3.582×10^{-3}		3.626×10^{-3}		7.442×10^{-4}	

Figures 4-7 show the residuals versus time for first, second, third, and fourth order models of the Type 56 test zone excited by outdoor temperature only. The outdoor temperature record comprises 8760 hourly values from the Abu Dhabi TMY3 weather file.

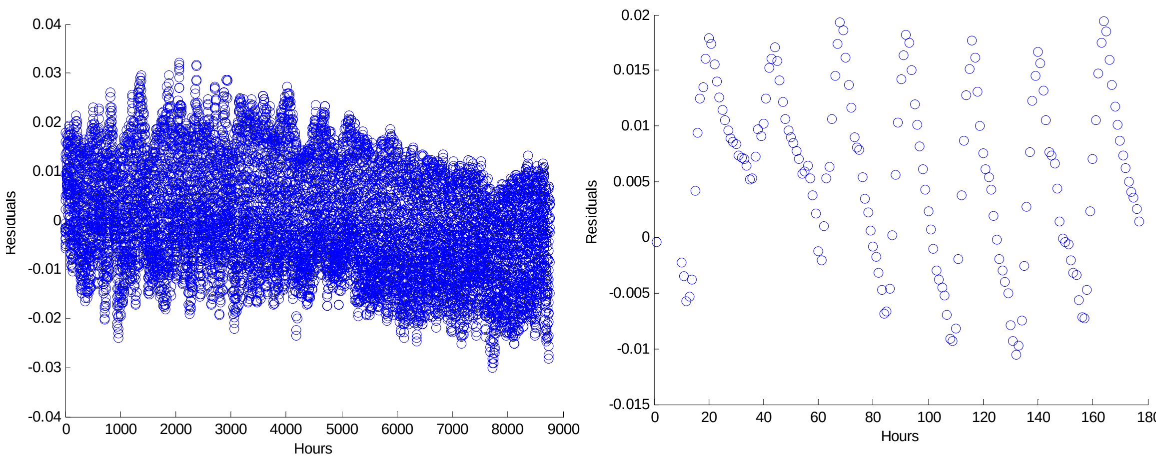

Figure 4: Residuals of First Order System (n=1) for One Year (Left) and for a Typical Week (Right).

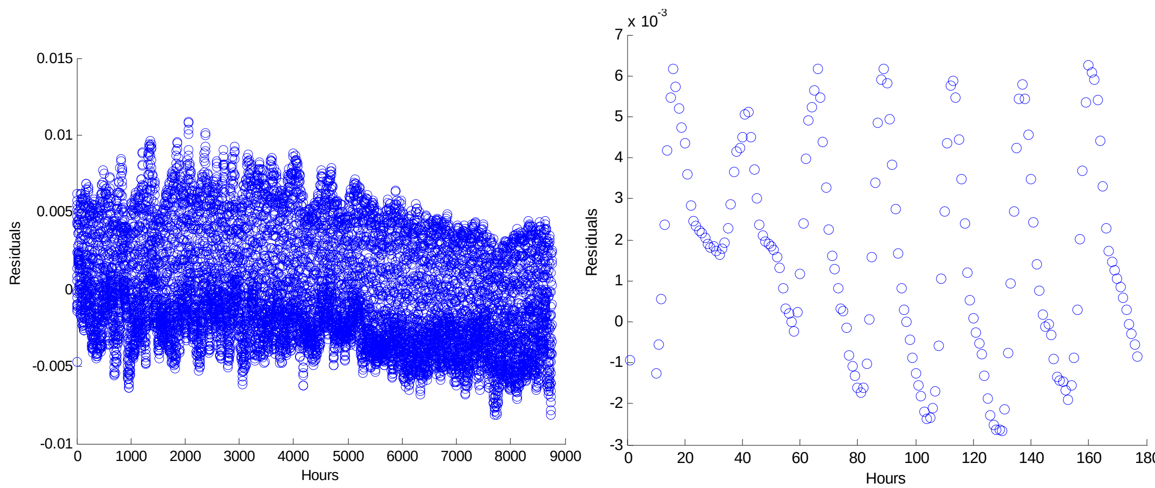

Figure 5: Residuals of Second Order System (n=2) for One Year (Left) and for a Typical Week (Right).

When fitting a reduced order model to simulated data one cannot expect a structure-free (white noise) residual vector. We see in the residuals correlation with the forcing functions and serial correlation as well. The only metrics that are meaningful interest for model-to-model exercises is the RMS of residuals and the t-statistics. Moreover, for ARMAX models, low t-statistics are acceptable for individual terms of the same variable with different lags provided the variable has significance for at least one of the lags, k=1:N. This behavior is seen consistently in the exterior walls where the 0- and 1-lag terms have low t-values. We retain these terms because they have physical meaning and removing them is known to bias the remaining coefficients.

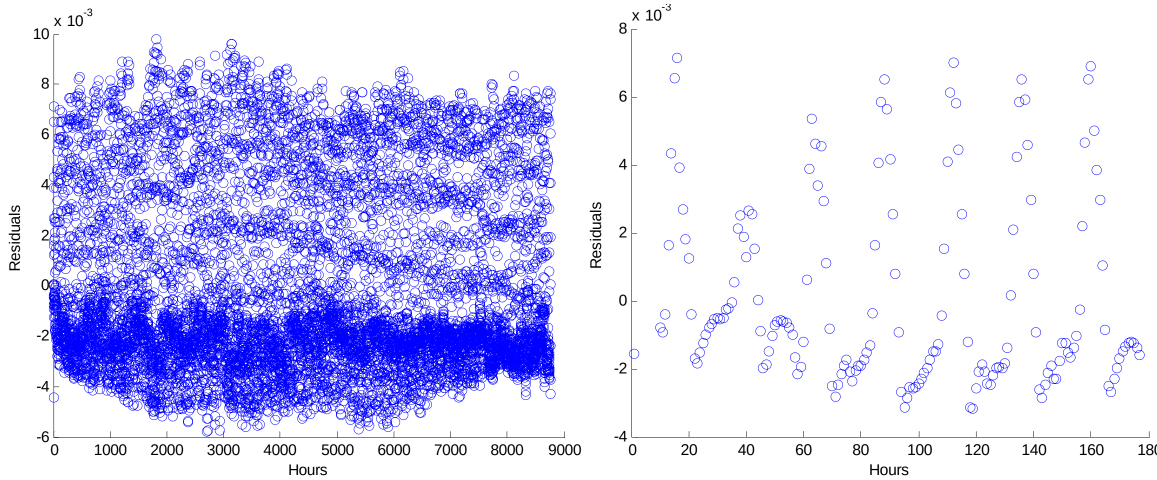

Figure 6: Residuals of Third Order System (n=3) for One Year (Left) and for a Typical Week (Right).

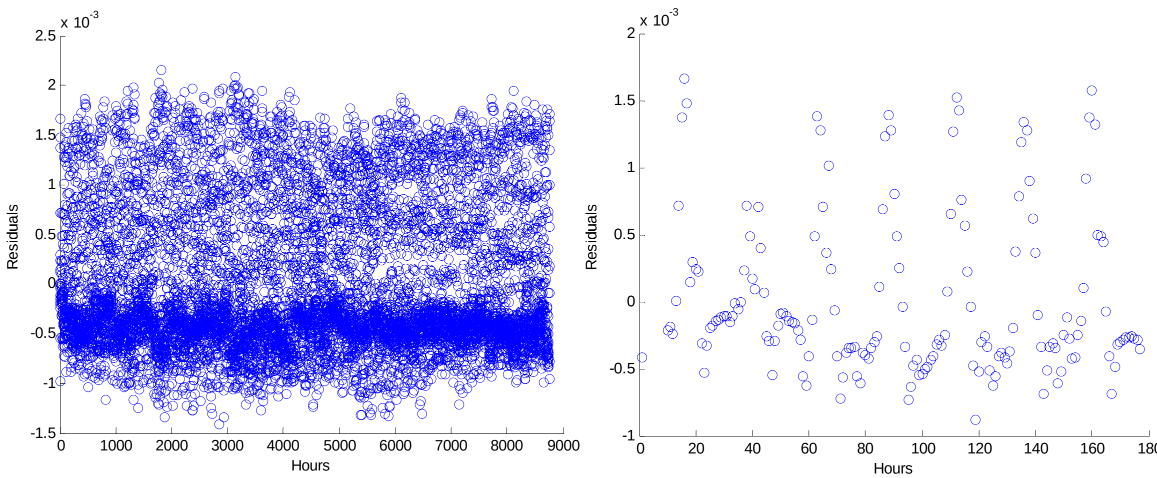

Figure 7: Residuals of Fourth Order System (n=4) for One Year (Left) and for a Typical Week (Right).

One unexpected result is the change in RMSE from 2nd- to 3rd-order model—there is none. However the residuals structure shows a distinct change—for 2nd-order model the residual span -3 to 7mK almost uniformly whereas the span increases slightly but a larger fraction of residuals cluster between 0 and -3mK for the 3rd-order model.

The constraint for positive real time constants can be applied to the same CRTF form using the same time-series data generated by the same TRNSYS procedure. The time constant work is underway.

RESEARCH 3: COOLING PLANT MODEL

A model of cooling plant performance is needed in terms of load and operating conditions. Latent cooling is assumed to be handled efficiently by DOAS with efficiently modulated variable refrigerant flow. Sensible precooling and direct sensible cooling are subject to a wide range of lift. Therefore both evaporating and condensing temperatures must be properly modeled.

Much work has been done on chiller modeling from experimental data. For more details and an extensive model see Zakula 2012. Many models incorporate a non-physical approach, fitting data with arbitrary constants that do not have physical meaning. The aim of this model is to create an accurate chiller representation requiring minimal solving time while grounding the solution in physically meaningful variables that could theoretically be measured for a given chiller.

In the model proposed, there are four inputs:

- T_x (Outdoor temperature)
- T_z (Indoor temperature)
- x (Capacity fraction)
- $Q_{e\max}$ (Rated capacity)

T_x was varied from 20-45°C, x was varied from 0.1-1, and Qe_{max} was provided at 3kW. Zone temperature T_z was varied from 15-30°C. For each capacity fraction and outdoor temperature, the model calculated a condenser and evaporator temperature proportional to approach temperature and pressure drop via capacity fraction:

$$T_c = T_x + x * dtccap + x^2 * d2tccap$$
$$T_e = T_z - x * dtecap - x^2 * d2tecap$$

in which *dtccap* and *dtecap* are the condenser and evaporator approach temperatures, and *d2tccap* and *d2tecap* are additional condenser and evaporator losses due to refrigerant-side pressure drops. The foregoing effective condensing and evaporating temperatures are used to determine compression work based on Carnot efficiency:

$$W = Q_e\left(1 - \frac{T_e}{T_c}\right)$$

where $Q_e = xQ_{e,max}$ is the cooling capacity (rated capacity multiplied by capacity fraction). Losses due to stator resistance (*Rcmpr*) and IGBT (*pm0* and *pm1*) are added to the compression work to obtain electrical work:

$$W_e = W + W^2 * Rcmpr + pm0 + pm1 * W$$

The electrical work is divided by the cooling capacity to obtain specific power, 1/COP. The resulting performance map is shown in Figure 8.

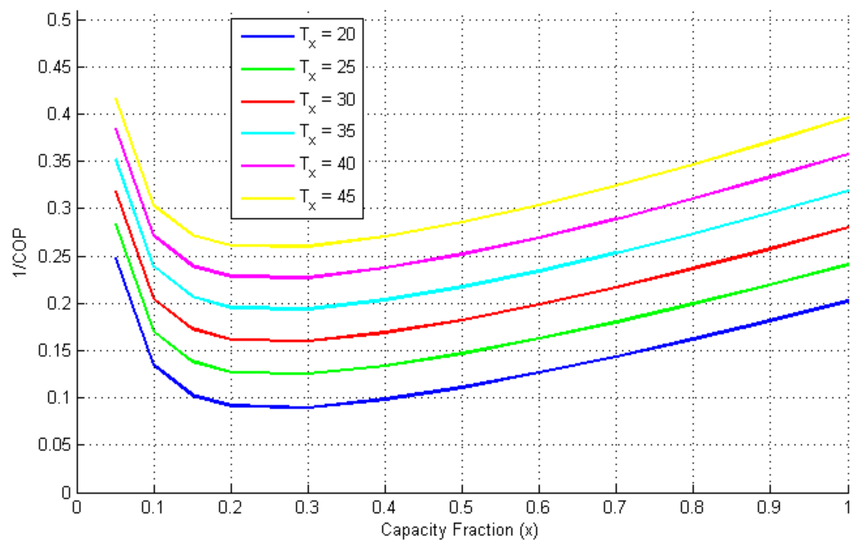

Figure 8: 1/COP v. Capacity Fraction of Final Model in Table 2. for T_z = 21°C and T_x = [20:5:45]°C.

The model coefficients were determined based on a 300 point data set generated from a deterministic heat pump model of a Mitsubishi split-type air conditioner with a single variable-speed rotary-piston compressor operating with R410a (Zakula 2012). The equations and the seven unknown parameters were solved with the Microsoft Excel Solver Add-In. The solutions were obtained with different constraints, e.g. in some cases a coefficient was forced to be non-negative or to a minimum positive value. A table of the various models and conditions sorted by RMSE is shown in Table 2.

Table 2: Model Coefficients for Various Constraint Combinations.

RMSE	dtecap	dtccap	Rcmpr	pm0	pm1	d2tecap	d2tccap	Conditions
0.0085	-460.8407	496.5068	7.6706	0.0352	1.0806	0	0	No Constraints
0.0089	-442.0947	476.5311	7.0342	0.0350	1.1269	0.5	0.5	Different IG
0.0133	0	25.9789	0.5379	0.0368	1.1489	0	0	>=0
0.0136	8.5685	17.1371	1.0086	0.0369	1.1438	--	--	Diff. Constraints

As shown from the table, a model with no coefficient constraints outperformed those with constraints in terms of RMSE. However, the models with less error exhibit negative coefficients, a physical impossibility. The constraints (or lack thereof) can have a large effect on the model coefficient estimates – e.g. resulting in non-physical coefficient estimates in some cases.

Removing the terms that varied with the square of the capacity (*d2tecap* and *d2tccap*) and applying the constraint:

$$dtecap \geq \frac{dtccap}{2}$$

resulted in a model formulation with physically reasonable parameters with comparable RMSE as the other physically realizable parameter set. Residuals for this reduced order model—the last listed in Table 2 – are shown in Figures 9 and 10. Refinement of the low-order chiller model is ongoing.

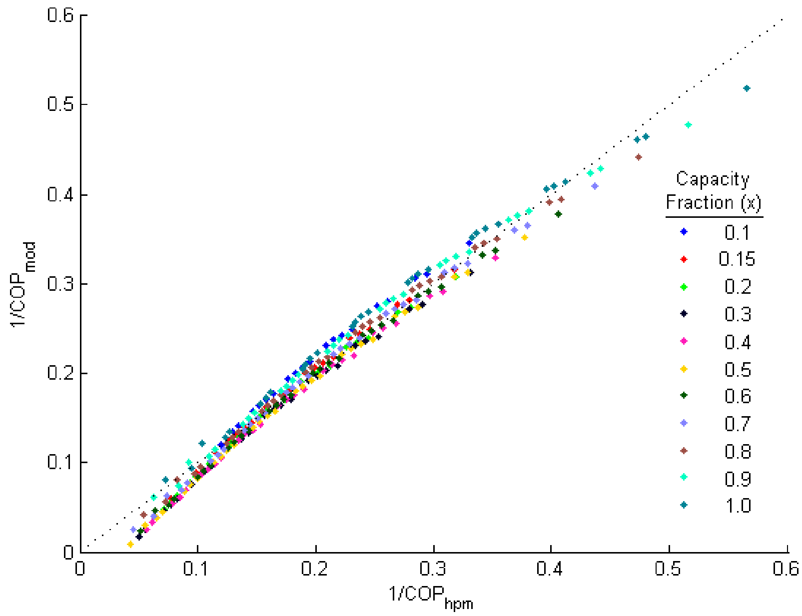

Figure 9: Model Predicted 1/COP versus deterministic heat pump model data. Colors correspond to capacity fraction.

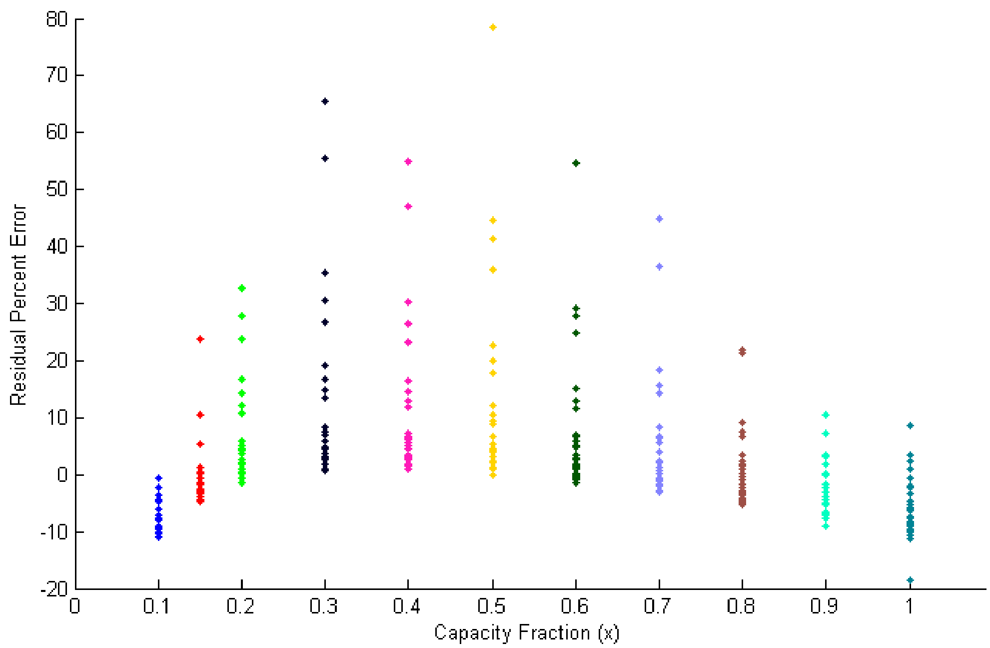

Figure 10: Residual percent error versus capacity fraction. Note that 1/COP is badly over-predicted for some conditions. High and low capacity fractions exhibit the tightest residual groupings, while middle fractions have wider spread of COP error.

RESEARCH 4: PREPARATIONS FOR LIVE MPC TEST

Masdar Field Station (MFS) is selected as the building for initial development of forward and reverse CRTF models. It is a building of 470m^2 floor area and is oriented 52°North of West to minimize direct beam solar radiation incident on windows. The building has the following significant features:

- A highly insulated advanced façade which lowers the heat gain to the building and prevents any direct normal radiation (DNI) from entering the zone spaces
- Chilled water piping in the floor and ceiling for testing of hydronic radiant cooling system
- Daylighting system consisting of two parabolic dishes on the roof of the building which brings day light into the building for reduction of lighting loads during the day

Building layout, floor and façade details:

Figure 11 provides the zones layout of the building. The zones of interest which will be used for CRTF modeling are shown in blue. The floor slab piping, as set just before pouring the concrete, is shown in Figure 12.

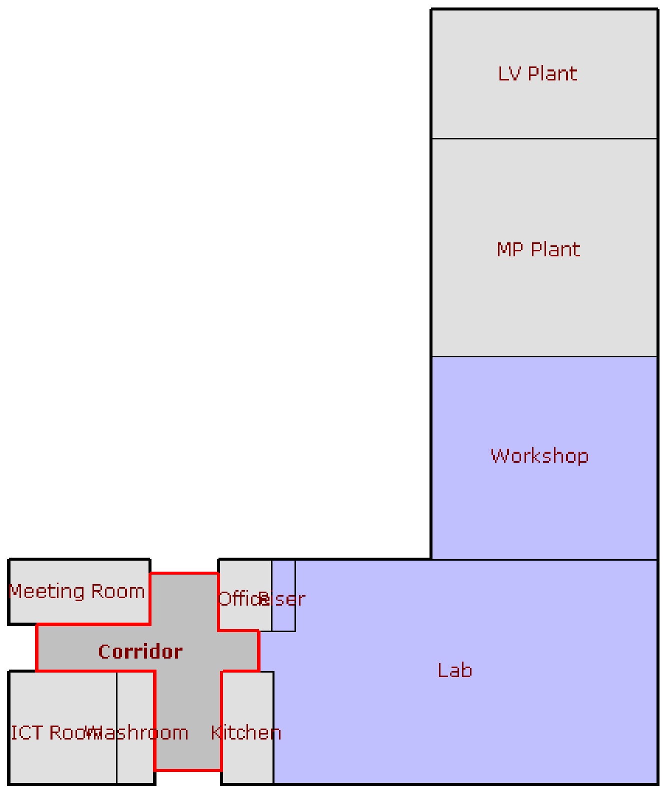

Figure 11: MFS Building Zones Description.

Figure 12: TABS Installation in Floor. Two lab zones are bounded by the red-white tapes; shop zone behind and left of 2nd tape; 4 ~200m loops per zone. Note coiled PEX hanging from completed ceiling slab.

The thermal features of the building façade based on the design values provided by the consultant are summarized in Table 3.

In order to reduce ground coupling and heat loss from the edges of the slab, polystyrene foam boards are placed beneath the floor slab and on the edges. The windows are located at three levels and consist of fixed external fins that prevent any DNI from entering the zone spaces as shown in Figure 13:

Table 3: MFS Building Facade Design Parameters.

External Wall U-Value (W/m^{2}K)	**0.25**
External Roof U-Value (W/m^{2}K)	0.12
Ground floor U-Value (W/m^{2}K)	0.35
U-Value of glass (W/m^{2}K)	1.2
U-Value of Frame (W/m^{2}K)	2
% of Glass to Wall (%)	30
G-Value (Glass) (-)	0.25
G-Value (Shaded) (-)	0.15
% Light Transmission (%)	50
Infiltration Working/non-working (ACH)	0.15/0.05

Figure 13: MFS NE elevation. Note windows shaded by external fins and daylighting parabolic dishes on roof.

There are two staircases located on the southeast and southwest ends of the building for accessing the roof area. There are two glass doors, six steel doors and two rolling shutter doors in the building. The two parabolic dishes shown in Figure 13 bring in daylight to the lab space to reduce lighting load.

TRNSYS MFS ENERGY MODELING:

Initially the MFS building thermal load model was developed in eQuest for the purpose of estimating the peak load as part of another research project. eQuest is considered as the industry standard for doing building energy simulation because it is freely available and has the power of DOE2 simulation engine. However, eQuest does not have the flexibility of exciting each zone with the desired impulse magnitude to observe simulated impulse response. Therefore, TRNSYS was selected for generating the data required for CRTF modeling. Figure 14 shows the 3D TRNSYS model of the MFS made in SketchUp using the TRNSYS 3D plugin.

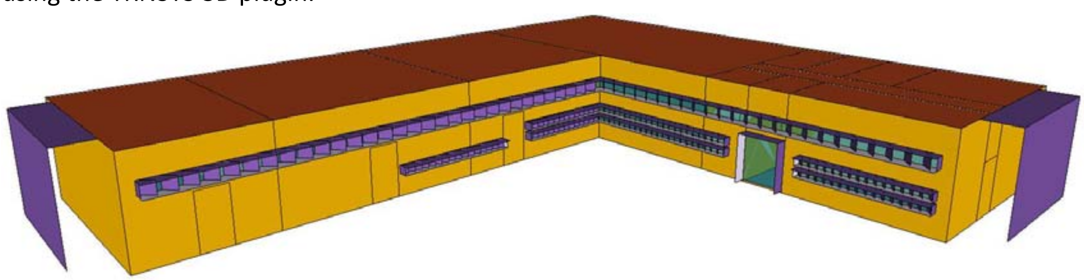

Figure 14: 3D TRNSYS model of the MFS.

The TRNSYS model consists of the zones as mentioned in Figure 11. The corridor zone is further divided into three zones so that all the zones are concave i.e. every wall can see the other wall in the zone as required by the enclosure radiant exchange model of TRNSYS type 56 multi-zone building model.

Model approximations and Internal Gains details:

- The staircases are modeled as shading devices as shown in Figure 14.
- Window data having the closest G-value, U-value and visible transmission as mentioned in Table 3 is chosen from the TRNSYS window library.
- The external fins having a 12mm bulge in the center are approximated by a rectangular shading surface of equal area to minimize the computing time of simulation.

- The walls are roof are modeled using layer by layer construction based on the section details provided by the consultant. However, due to unavailability of as-built material properties, standard material libraries are used to approximate the U-values provided in Table 3.
- The ground coupling and slab edge loss are modeled by adding an extra fictitious layer of insulation as shown in Figure 15 whose U-value is computed using the eQuest model of MFS (McDowell, Thornton, and Duffy 2009).

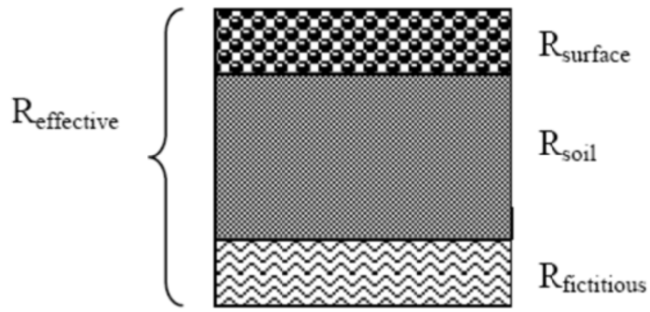

Figure 15: DOE2 Slab Edge-Loss Modeling Approximation.

- The schedules for building occupancy, lighting and electrical gains are based on Masdar Energy Design Guildlines (MEDG) 3.0 appendix E (*Masdar Energy Design Guidelines (MEDG) for New Buildings* 2011). Table 4 describes the gains used for modeling internal gains.

Table 4: MFS Zones Internal Load Details. Last column is sum of Infiltration and Ventilation.

Space Name	Area (m^2)	Volume (m^3)	No. of People	cfm/ person	SHGain (W)	LHGain (W)	Lighting (W/m^2)	Ltg Radtn %	Eqpt. (W/m^2)	(cfm/m^2) (ACH)
ICT Room	22.443	98.164	0	5	73.268	58.614	8.934	0.67	53.82	1.287 (0.5)
Washroom	11.844	51.807	2	50	73.268	73.268	17.115	0.67	7.535	8.556 (3.32)
Mtg Room	19.845	86.803	6	25	71.802	45.426	29.708	0.67	64.58	7.427 (2.88)
Office	6.54	28.623	2	25	73.268	58.614	15.285	0.67	64.58	7.667 (2.98)
Kitchen	10.57	46.234	2	33	80.595	139.209	18.944	0.67	86.11	6.259 (2.43)
Lab	149.139	652.33	10	25	73.268	58.614	13.240	0.67	53.820	1.691 (0.66)
Workshop	79.532	428.535	5	25	73.268	58.614	13.240	0.67	53.820	1.578 (0.61)
MP Plant	84.995	381.233	1	5	73.268	73.268	3.552	0.67	21.528	0.059 (0.02)
LV Plant	50.692	231.361	1	5	73.268	73.268	3.552	0.67	21.528	0.099 (0.04)
Corridor	15.216	66.557	1	25	73.268	73.268	10.764	0.67	53.820	2.575 (1)
Door North	10.2	44.615	0	0	72.095	48.650	10.764	0.67	62.032	2.567 (1)
Door South	5.61	24.534	0	0	72.095	48.650	10.764	0.67	62.032	2.571 (1)

Note: ACH of 0.5 is considered for ICT room and ACH of 1 for corridor zones

Comparison between eQuest and TRNSYS model:

TRNSYS and eQuest building thermal load models produce different peak load estimates when excited by the same weather data. To obtain similar results the following must be addressed:

- Windows can be defined using layer-by-layer method which can incorporate shading devices such as external fins natively in eQuest while this option is not available in TRNSYS. We are currently working on to create the desired window data through software "WINDOW 7" developed by Lawrence Berkley National Laboratory (LBNL) which can be used to create the desired window data which can be used by eQuest and TRNSYS.
- Only concave zones can use detailed radiation model in TRNSYS which requires change of zone description in the eQuest model as shown in Figure 11.
- TRNSYS type 56 doesn't have the capability to model recessed windows and doors directly. Currently we use shading surfaces around windows in TRNSYS to create the recessed window effect.

MFS Building Management System (BMS):

The MFS BMS is based on the BACnet protocol and consists of the following systems relevant to this project:

- Chilled Water (CHW) system
- CHW Fan Coil Units (FCU) (7)
- Hot Water (HW) system
- Air Handling Unit (AHU) with Enthalpy Recovery
- Demand Controlled Ventilation System
- Thermal Energy Meters (9)
- Electrical Power Meters (27)

The building is cooled by a water-cooled chiller which supplies CHW to the FCU's, AHU, hydronic radiant cooling piping in the floor and ceiling and domestic cold water heat exchanger (HX). The FCU's are fitted with variable speed fans with the diffusers located beside it resulting in low fan static pressure and increased efficiency.

The AHU is designed to provide 100% outdoor air to the building at desired supply air temperature and humidity. It uses an enthalpy recovery heat wheel to recover energy from the return stream. A cooling coil located after the recovery wheel fed by CHW from the chiller is used for supply air dehumidification. A heating coil located after the cooling coil fed by hot water from the domestic calorifier adjusts the temperature to the desired building supply air set-point. The supply and return fans are controlled to maintain a desired set-point pressure in the supply air duct.

The amount of supply air fed to the lab and workshop zones shown in Figure 11 is controlled by an air quality system that monitors the temperature, relative humidity, CO_2 and total volatile organic content (TVOC) of the zone air and commands a volume control device to maintain desired set-point for the parameter closest to violating its setpoint. A separate hazardous extract system is also present in the building. The hazardous extract points within the test zones will be sealed during CRTF excitation experiments.

The thermal energy meters monitors the cooling and heating energy supplied to the building. They are installed at the following CHW and HW circuits of interest:

- Primary CHW circuit
- hydronic radiant cooling CHW circuit
- FCU CHW circuit
- Domestic cold water HX
- AHU CHW circuit
- Domestic HW circuit
- AHU HW circuit
- Condenser water circuit

Currently, the BMS reads only energy output from the thermal energy meters in forms of pulse signals generated for every 10kWh of energy. Work to connect the meters to the BMS using serial MODBUS signals is underway in order to obtain higher resolution and to also record volumetric flow rate and hot and cold-side temperatures from each thermal energy meter.

The electrical power supplied to the building systems is monitored by 24 electrical energy meters. Multiplier and reverse CT errors have been corrected. Four of the 24 remain to be properly configured.

The parameters of interest from the above systems are logged by using a third party historian which gathers the data from the BMS and stores in the Microsoft cloud for easy access.

Air Tightness Testing

The air tightness testing performed to date includes baseline testing for the lab and workshop doors. Air tightness testing for the workshop zone is ongoing, especially efforts to identify leak sites and seal the leaks. Air leakage testing for the workshop and lab is done separately to accurately characterize the latent load for each zone.

Figure 16 shows the orientation for lab and workshop door leakage testing.

Figure 16: Air Leakage Testing - Lab and Workshop Doors.

Baseline results for lab and workshop door testing are shown in Table 5.

Table 5: Lab and Workshop Door Leakage Testing.

Test Results	Lab Door	Workshop Door
Air Flow @ 50 Pascal	195 CFM	95 CFM
	493.47 ACH	106.65 ACH
Leakage Areas:		
Canadian EqLA @ 10Pa		11 in^2
LBL ELA @ 4 Pa	10.7 in^2	6.2 in^2

195 CFM and 95 CFM (Cubic feet per minute) @ 50 Pascal is the air flow from the blower door fan to create a change pressure over the door (lab and workshop) of 50 Pascal. Depressurization testing was performed on the separate spaces. 50 Pascal pressure is equivalent to pressure generated by a 20mph wind blowing from each side of the building (The Energy Conservatory, 2012). CFM50 is a commonly used measure of building airtightness and provides an indication of the total air leakage in the building envelope (The Energy Conservatory, 2012). 493.47 air changes per hour (ACH) and 106.65 ACH provides information when the entire volume of air in the building is replaced at 50 Pascal pressure. Equivalent

leakage Area (EqLA) and Effective Leakage Area (ELA) provide a leakage estimate at 10 and 4 Pascal, respectively. Both of these estimates are based on different assumptions about the physical shape and behavior of the leaks. Details can be found in the Minneapolis blower door manual (The Energy Conservatory, 2012). 10.7 in^2 and 6.2 in^2 provide information on the leakage area on the lab and workshop doors, respectively. Efforts were further made to seal the infiltration points by using door sealing strips, and the comparison results shall be presented in the next quarter report.

Thorough air leakage testing was also performed on the workshop zone. Following are the steps carried out to date:

- Baseline condition established for the workshop zone without any sealing. The inside and outside rolling doors were closed.
- Fresh air and exhaust ducts were sealed in the workshop area.
- Outside rolling door was sealed with plastic sheet and duct tape.
- Inside rolling door was sealed with plastic sheet, testing is ongoing.

All the seals were carefully tested with a smoke pen. Orientation of the cases completed to date for the workshop zone are shown in Figure 17.

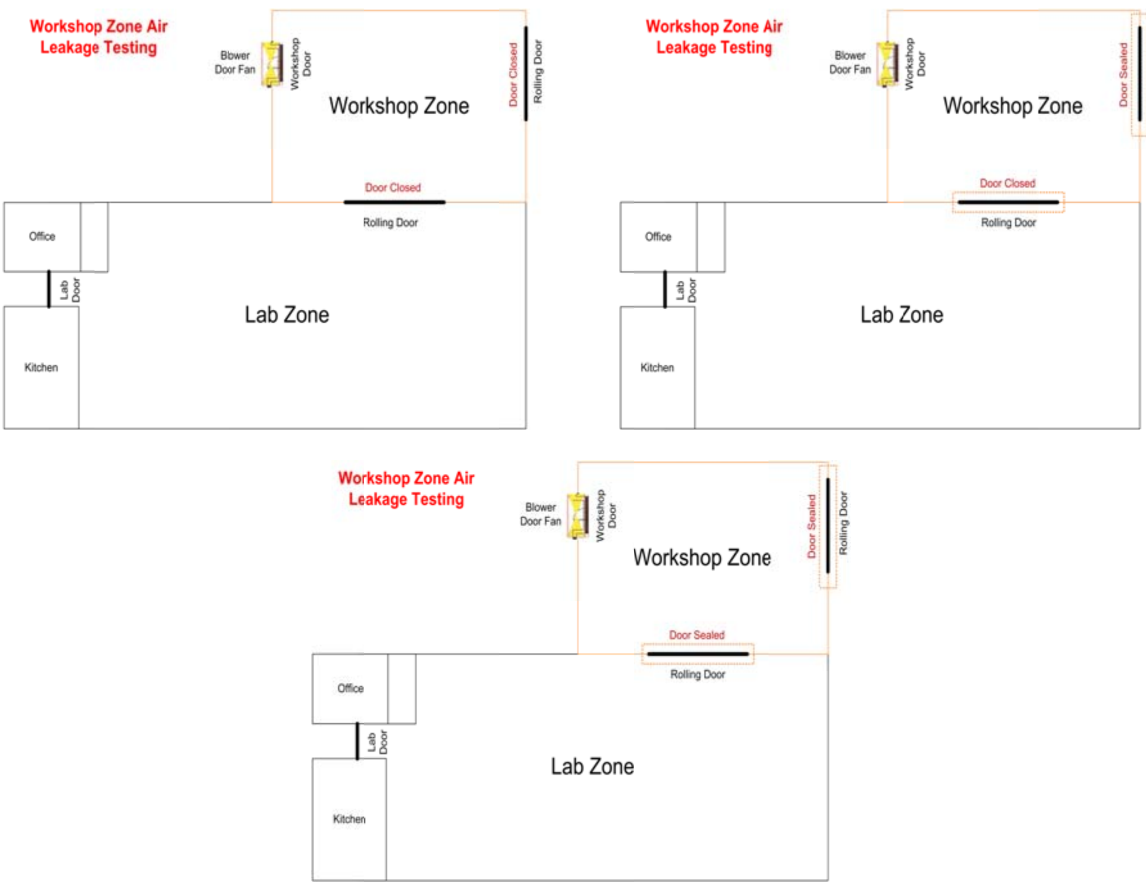

Figure 17: Air Leakage Testing (With and Without Sealing) - Workshop Zone.

Leakage testing results for the workshop zone for the above mentioned cases (Figure 17) is shown in Table 6.

Table 6: Workshop Zone Leakage Testing Results.

Test Results	**Workshop Baseline (without any sealing, only rolling door closed)**	**Workshop outside (rolling door sealed)**	**Workshop Inside (rolling door sealed)**
Air Flow @ 50 Pascal	1615 CFM 7.88 ACH	1542 CFM 7.53 ACH	1376 CFM 6.72 ACH
Leakage Areas:			
Canadian EqLA @ 10Pa	184.0 in^2	160.7 in^2	152.8 in^2
LBL ELA @ 4 Pa	103.6 in^2	86.0 in^2	84.8 in^2

Table 6 shows that leakage area estimates are reduced from 103.6 in^2 to 84.8 in^2 @ 4 Pascal as the air infiltrations are sealed in the workshop. Further efforts will be made in the next quarter to decrease the leakage area estimates to the best practice values found in high performance buildings.

2Q Summary (10 July 2013 to 31 January 2013)[PA1]

A general formulation of the demand response problem involving cool storage in the building structure has been developed. Two transient thermal response models are embedded in the general formulation, one for the occupied zone and one for TABS element connected with that zone. A method of estimating a comprehensive room transfer function (CRTF) from the TRNSYS zone model has been developed.

The model identification procedure will be tested in the *Masdar Field Station* (MFS). Efforts are underway to upgrade the control system (BMS) of the MFS, characterize the building's leakiness and transient thermal response, and modify parts of the air and hydronic distribution systems. eQuest and TRNSYS models of the MFS have been developed.

A new low-order representation of heat pump and chiller performance has been formulated and tested using performance maps generated by detailed simulation. The representation is based on first principles models of irreversibilities in heat transfer, fluid transport, and electro-mechanical (motors, drives) subsystems. The possibility of identifying reliable performance functions with very few chiller (or heat pump) test points will be explored.

References

Seem, J. E. (1987). *Modeling of Heat Transfer in Buildings*. Doctoral dissertation, Mechanical Engineering, U. Wisconsin.

Armstrong, P. R., Leeb, S. B., & Norford, L. K. (2006). Control with building mass. *ASHRAE Transactions*, 112, Part 1.

Masdar Energy Design Guidelines (MEDG) for New Buildings. 2011. Masdar City Energy Department.

McDowell, T. P., J. W. Thornton, and M. J. Duffy. 2009. "Comparison of a Ground-Coupling Reference Standard Model to Simplified Approaches." In *Eleventh International IBPSA Conference, Glasgow, Scotland*. http://www.ibpsa.org/proceedings/BS2009/BS09_0591_598.pdf.

Potter, Martyn (MI Director of Facilities), 2013. Personal communication 2013.02.05.

Seem, J. E., and J.E. Braun (1991). Adaptive methods for real-time forecasting of building electrical demand. *ASHRAE Transactions*, 97(1):710–721.

The Energy Conservatory, 2012. *TEC Blower Door Operation Manual*.

Zakula, T., P.R. Armstrong and L.K. Norford, 2012. Optimal coordination of heat pump compressor and fan speeds and subcooling over a wide range of loads and conditions, *HVAC&R Research* 18(6):1153-67

Publications/Presentations

None

Appendices

None